Electrical Power and Energy Systems 78 (2016) 165–173

Contents lists available at ScienceDirect

Electrical Power and Energy Systems

journal homepage: www.elsevier.com/locate/ijepes

Modeling, control and analysis of cascaded inverter based grid-connected photovoltaic system

Nayan Kumar *, Tapas Kumar Saha, Jayati Dey

Department of Electrical Engineering, National Institute of Technology Durgapur, Durgapur 713209, India

ARTICLE INFO

Article history:
Received 2 March 2015
Received in revised form 21 November 2015
Accepted 25 November 2015

Keywords:
Photovoltaic system
Cascaded two-level inverter
Vector control
Static compensator (STATCOM)

ABSTRACT

This paper proposes a vector controlled isolated source cascaded two-level inverter (CTLI), for grid connected photovoltaic (PV) system. The system is controlled to operate with variable solar irradiance, supplying different levels of active power. The PV systems are designed, modeled and tested with the proposed controller, to provide maximum power output. Additional operation as a reactive power supplier, in the absence of solar radiation, is also tested. A simple sinusoidal pulse width modulation (PWM) technique is used, instead of referred space vector PWM (SVPWM) technique, for the operation. Two different schemes have been considered to operate the inverter with equal and unequal DC-link voltages. The control scheme has been found working, for both active and reactive power supply in steady state and transient conditions. The power supplies of both the schemes are analyzed. The controller performance is found to be satisfactory for both the schemes to extract maximum power at the considered working conditions.

Introduction

The grid-connected PV system is one of the best options, for sustainable and independent energy generation practice. The power electronic technology plays an important role in the distributed generation and integration of renewable-energy sources into the electrical grid [1]. Many grids connected PV systems [26], use a three-phase voltage source inverter [2–4]. However, the conventional three-phase inverter produces three output voltage levels, and has poor spectral performance in lower switching frequency. The number of levels can improve the spectral performance at lower switching frequency. There are other attractive features, which make these kinds of power converters very interesting for the power industry, like (i) reduced current and voltage harmonics on the AC side, (ii) high-voltage capability, and (iii) low dv/dt [5–10]. Several multilevel topologies used for grid connection have been proposed in [5–9,11]. Multilevel converter structures have three major classifications; (i) neutral point clamped (NPC) or diode clamped, (ii) flying capacitor (FC) or capacitor clamped, and (iii) cascaded H-bridge (CHB) inverter, with isolated DC source [10,12]. The CHB inverter topology is very much popular because of its modular circuit layout [13]. The CHB topology requires the lesser number of DC-link capacitors than other topologies. The control of individual DC-link voltage of the capacitors is difficult [14]. The topology consists of two inverters connected to the open winding primary of a three-phase transformer.

In this work, the DC-link voltages of both the inverters are chosen to be in the order of battery voltage. The PV modules are connected at the DC-links of the CTLI. Accordingly, the PV modules are designed to deliver maximum power at that DC voltage, under rated Indian solar irradiance. A novel control strategy is developed to control the active power flow of the total DC-link voltage of two inverters. The circuit-based model of a PV array that can be implemented in any simulation environment is proposed in [15]. In the present study, single diode model of solar cell is used following the equations developed in [16].

DC/DC converters, connected to the DC-link capacitors, usually control the variations of output voltage of PV systems [5]. Various control strategies are available in literature to control the converters [5–10,14,17,18]. In [13], one control technique is proposed to keep the DC-link voltages constant for the isolated sources by balancing the active power flow. However, different level of DC-link voltages, which is favored because of certain harmonic reduction, and the maximum power generation by the different PV modules are beyond the scope of it. Accordingly, this paper proposes two schemes with equal and unequal voltage levels for the considered inverters for different solar irradiance level. The variation in solar irradiance level has to be introduced for checking the performance of the controller [20,27]. The PV modules of different voltage levels

* Corresponding author.
E-mail address: nayansays@gmail.com (N. Kumar).

http://dx.doi.org/10.1016/j.ijepes.2015.11.092
0142-0615/

Nomenclature

V	solar cell terminal voltage [V]
I	solar cell terminal current [A]
I_{ph}	photo generated current [linear with irradiance]
I_s	saturation current due to diffusion mechanism
T	cell temperature [K]
K	Boltzmann's constant $[1.38 \times 10^{(-23)}$ J/K]
q	electron charge $[1.6 \times 10^{-19} C]$
n	diode quality factor [silicon diode $n = 2$]
R_s	cell series resistance [Ω]
R_{sh}	cell shunt resistance [Ω]
N_P	number of parallel cells
N_s	number of series cells
M	PV identical modules per string
N	identical PV strings
V_{dc}	DC-link voltage of the voltage source inverter (VSI)
V_{a1}, V_{b1}, V_{c1}	first inverter pole voltages
V_{a2}, V_{b2}, V_{c2}	second inverter pole voltages
$L-N$	line to neutral
V_q	q-component of the source voltage
V_d	d-component of the source voltage
e_d	d-components of the transformer output voltage
e_q	q-components of the transformer output voltage
i_d	d-components of the transformer output current
i_q	q-components of the transformer output current
V^*_{dc}	reference DC-link capacitor voltage of inverter
R_L	resistive load

are developed in this work. Two separate vector controller have been developed in this study for the two schemes. In both the cases, the proposed control technique maintains the total DC-link voltages of two inverters. Initially, the solar irradiance for the two inverters is considered to be same. Afterwards, the input is allowed to vary for each solar module separately. This variation in solar irradiance for the two PV modules of a single system is made to check even a difficult operating situation. The complete power circuit has been depicted in Fig. 1.

The paper is organized as follows: In the Section "Definition of the problem", definition of the problem is described. Section "Mat hematical model of a photovoltaic cell" presents a mathematical model for the photovoltaic cell. Section "Modeling of grid connected CTLI", illustrates the grid-connected CTLI topology and its modeling. The system description is given in Section "System description". Results followed by discussion are presented in Sections "Simulation result", "Reactive power control", and "Output power and efficiency of the schemes", respectively. Finally, the conclusions that have been drawn from the present work are summarized in Section "Harmonic analysis of the schemes".

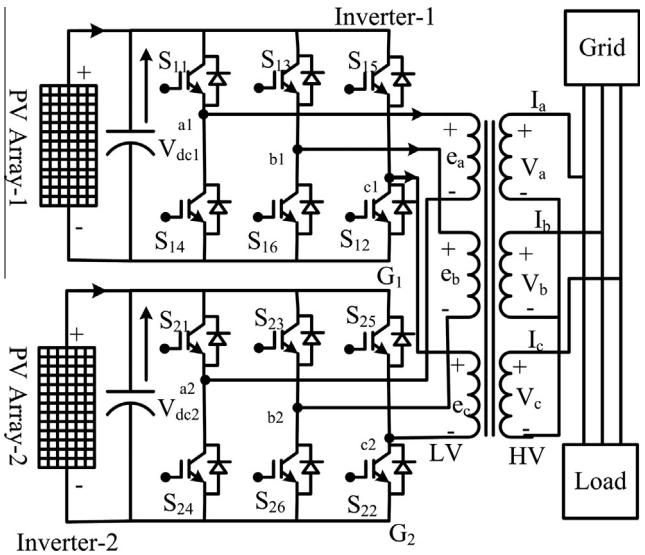

Fig. 1. Power circuit of the photovoltaic system with cascaded two-level inverter.

Definition of the problem

Two isolated PV sources are connected through the inverters as shown in Fig. 1. A novel control scheme is proposed so that the cascaded two-level inverter (CTLI) based system would work under variable solar irradiance levels and also in the absence of solar irradiance (as distributed static reactive power compensator). Two power schemes are studied, with the following nature.

I. Two inverters with same DC-link voltages
II. Two inverters with unequal DC-link voltages

To address the additional complexity of real-life variable solar irradiance, the inputs are considered to be different for two inverters as well. The solar irradiation is changed by ±17.133% in a step in the following manner.

(i) Solar irradiance of first inverter deviates as shown as Fig. 2 (a).
(ii) Solar irradiance of second inverter deviates as shown as Fig. 2(b).

The step changes of the input to the power schemes are introduced in simulation environment following [20,27]. Since the changes in solar irradiance acts as an exogenous input disturbance, it is customary to consider this change as a step signal which signifies for a worst-case perturbation in input from the control engineering standpoint.

The modulation technique for the CTLI is tested with a simple sinusoidal PWM technique instead of generally preferred SVPWM modulation technique.

Finally, the overall system efficiency and total harmonic distortion (THD), to extract maximum power from the PV modules, has been investigated for both the power schemes with the considered solar irradiation variation.

Mathematical model of a photovoltaic cell

A mathematical description of the characteristic of PV cells is developed based on [16,21]. The characteristic equation is given in (1).

$$I = I_{ph} - I_s\left[\exp^{\frac{q(V+IR_s)}{nKT}} - 1\right] - \frac{V + R_s I}{R_{sh}} \quad (1)$$

The equivalent circuit, determined from the equation, is presented in Fig. 3.

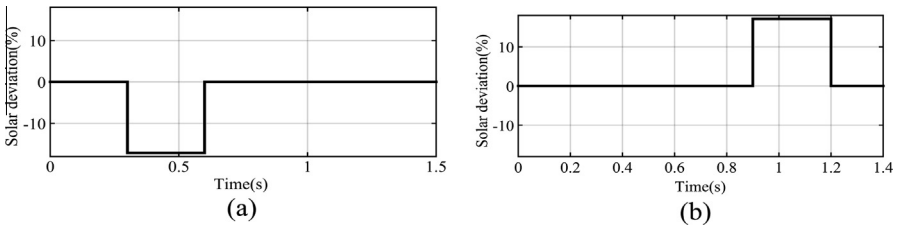

Fig. 2. Solar deviation from the nominal (a) the first inverter, connected to PV model-1, and (b) the second inverter, connected to PV model-2.

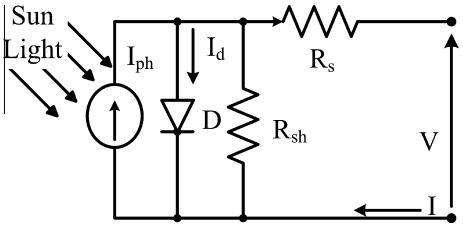

Fig. 3. Solar PV cell equivalent circuit.

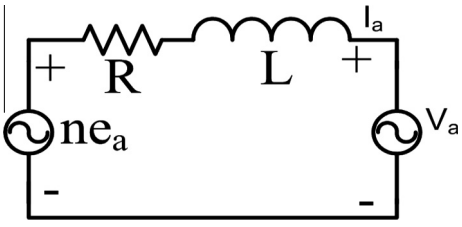

Fig. 5. Single phase equivalent circuit.

The parameter values of the model have been selected following the data given in [15]. PV modules can be assembled in series and/or parallel to build a PV array [16].

The complete multidimensional array model equation is:

$$I = N_p\left[I_{ph} - I_s\left(\exp^{\frac{q\left[\left(\frac{V}{N_s}\right)+\left(\frac{I}{N_p}\right)R_s\right]}{KT}} - 1\right) - \frac{\left(\frac{V}{N_s}\right)+\left(\frac{I}{N_p}\right)R_s}{R_{sh}}\right] \quad (2)$$

PV modules for the scheme-I

The number of series cells are chosen to provide maximum power at 48 V, at normal Indian solar irradiance for the scheme-I. Power rating of the inverter is 2.5 kW and one PV cell has $R_s = 0.4\,\Omega$, $R_{sh} = 323\,\Omega$ [8]. The N_s and N_p are calculated for this scheme and found to be 12, and 250 respectively.

The designed PV system output power at different output voltage has been depicted in Fig. 4(a). Here the output power is found to be the maximum at 48 V with normal Indian solar irradiance. Six similar PV modules are connected in parallel and developed one PV array. Two similar PV arrays are connected with two inverters following the scheme, presented in Fig. 1. It is found that the load voltage and power output curve are matching with the theoretical characteristics.

PV modules for scheme-II

Unequal DC-link voltages are chosen for the two inverters in the scheme-II. For seven level output voltage, the voltage ratio of the two-inverter DC-link sources is to be taken as 1:0.366 [14,19]. This ensures the reduction of $(6n+1)$ harmonic $(n = 1, 3, 5, 7, \ldots)$. In this paper, the DC-link voltage of the first inverter is maintained at 70.272 V whereas the second inverter has the same as 25.728 V. This maintains the total voltage at 96 V, which is same as that of the scheme-I.

In this scheme, the inverters are to be supplied with different types of PV arrays to maintain the voltages at the desired levels of 70.272 V and 25.728 V, respectively. The first inverter is sup-

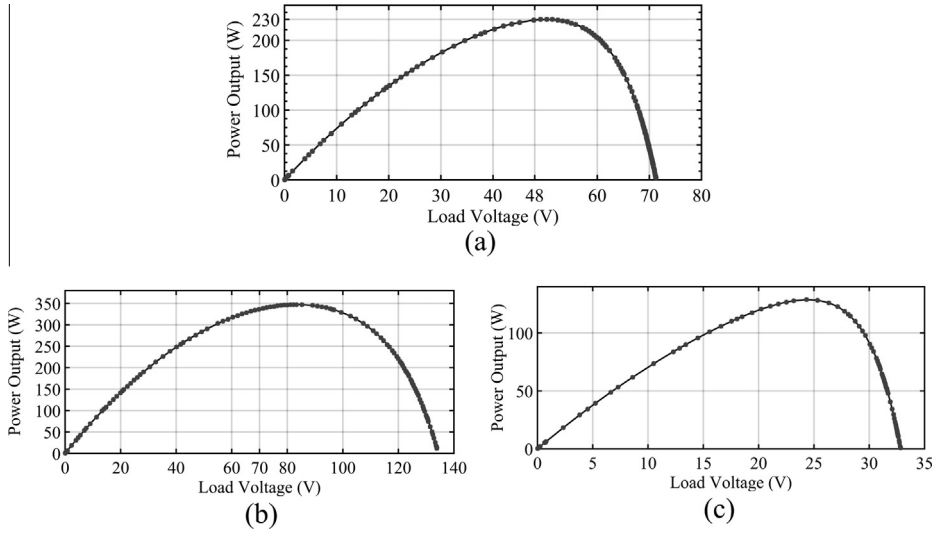

Fig. 4. Power–voltage characteristics for different values of load (R_L) for a PV system used in (a) the scheme-I (to provide maximum power at 48 V), (b) the scheme-II, Inverter-I (to provide maximum power at 70 V), and (c) the scheme-II, Inverter-II (to provide maximum power at 25 V).

plied by six parallel PV modules, having $N_s = 17$ and $N_p = 250$ in each of them. The output power–voltage (P–V) curve for one module has been presented in Fig. 4(b). The second inverter is supplied by PV modules, having $N_s = 8$ and $N_p = 250$. The output power–voltage (P–V) curve obtained from this module has been presented in Fig. 4(c).

The power–voltage (P–V) curves are showing the maximum powers are produced at around the desired voltage levels by the two different PV modules at a normal Indian solar irradiance.

Modeling of grid connected CTLI

For the considered power scheme, as shown in Fig. 1, the voltage across a, b, and c windings of the transformer are constructed as follows:

$$e_a = \frac{2}{3}(V_{a1} - V_{a2}) - \frac{1}{3}(V_{b1} - V_{b2}) - \frac{1}{3}(V_{c1} - V_{c2}) \tag{3}$$

$$e_b = -\frac{1}{3}(V_{a1} - V_{a2}) + \frac{2}{3}(V_{b1} - V_{b2}) - \frac{1}{3}(V_{c1} - V_{c2}) \tag{4}$$

$$e_c = -\frac{1}{3}(V_{a1} - V_{a2}) - \frac{1}{3}(V_{b1} - V_{b2}) + \frac{2}{3}(V_{c1} - V_{c2}) \tag{5}$$

where V_{a1}, V_{b1}, V_{c1} are the first inverter pole voltages, and V_{a2}, V_{b2}, V_{c2} are second inverter pole voltages. The output voltage levels of the scheme depend on the inverter DC-link voltages V_{dc1} and V_{dc2}. In this study; the inverters are initially considered to be operating with $V_{dc1} = V_{dc2} = 0.5V_{dc}$, and in the next scheme, the values are $V_{dc1} = 0.732V_{dc}$ and $V_{dc2} = 0.268V_{dc}$. In both the cases, the total DC-link voltage is considered to be same as $V_{dc} = 96$ V [14,19].

The first scheme produces output voltage with five levels, whereas the second one produces output voltage with seven levels. The harmonic spectrum is improved in the second scheme [14].

The equivalent circuit for 'a' phase of the transformer has been presented in Fig. 5. In the figure; V_a is the grid voltage; R is the resistance representing the loss in the system, and L is the leakage inductance of the transformer windings. The voltage across the primary of the transformer is e_a which is controlled by first and second inverter. The transformer is step-up with turn ratio 1:n.

Applying KVL for 'a', 'b' and 'c' phases

$$ne_a = R_a i_a + L_a \frac{di_a}{dt} + V_a \tag{6}$$

$$ne_b = R_b i_b + L_b \frac{di_b}{dt} + V_b \tag{7}$$

$$ne_c = R_c i_c + L_c \frac{di_c}{dt} + V_c \tag{8}$$

It is considered that R is equal to R_a, R_b and R_c and L are equal to L_a, L_b and L_c. Eqs. (6)–(8) can be rewritten as,

$$\frac{d}{dt}\begin{bmatrix} i_a \\ i_b \\ i_c \end{bmatrix} = \begin{bmatrix} -\frac{R}{L} & 0 & 0 \\ 0 & -\frac{R}{L} & 0 \\ 0 & 0 & -\frac{R}{L} \end{bmatrix}\begin{bmatrix} i_a \\ i_b \\ i_c \end{bmatrix} + \frac{1}{L}\begin{bmatrix} -V_a & n(e_a) \\ -V_b & n(e_b) \\ -V_c & n(e_c) \end{bmatrix} \tag{9}$$

The above equation is transformed to synchronously rotating reference frame. Due to this conversion, both active and reactive currents are decoupled and can be controlled independently. The V_d aligns with the synchronously rotating bus voltage vector. In this reference frame, the q-component of the source voltage V_q is found to be zero. The system model in the synchronous rotating reference frame is as follows:

$$\frac{d}{dt}\begin{bmatrix} i_d \\ i_q \end{bmatrix} = \begin{bmatrix} -\frac{R}{L} & \omega \\ -\omega & -\frac{R}{L} \end{bmatrix}\begin{bmatrix} i_d \\ i_q \end{bmatrix} + \frac{1}{L}\begin{bmatrix} e_d - V_d \\ e_q - V_q \end{bmatrix} \tag{10}$$

where e_d, e_q and i_d, i_q are d–q axes components of the transformer output voltage and current, respectively.

The objective of the system controller is to achieve voltage regulation of the inverter capacitors. This is accomplished by controlling the active and reactive power that flows into the grid. The d–q axis voltages can be written as:

$$e_d = (sL + R)i_d - L\omega i_q + v_d \tag{11}$$

$$e_q = (sL + R)i_q + L\omega i_d + v_q \tag{12}$$

The d–q axis currents are controlled by following Eqs. (11) and (12). The reference value of d-axis current is generated from the DC-link voltage controller. In this paper, the reference DC voltage is kept at 96 V. The reference current now can be written as:

$$i_d^* = \left[V_{dc}^* - (V_{dc1} + V_{dc2})\right]\left(K_{pdc} + \frac{K_{idc}}{s}\right) \tag{13}$$

The control scheme is shown in Fig. 6. Here the V_{dc}^* is the reference voltage, and V_{dc1}, V_{dc2} are the actual DC-link voltages of the first inverter and second inverter.

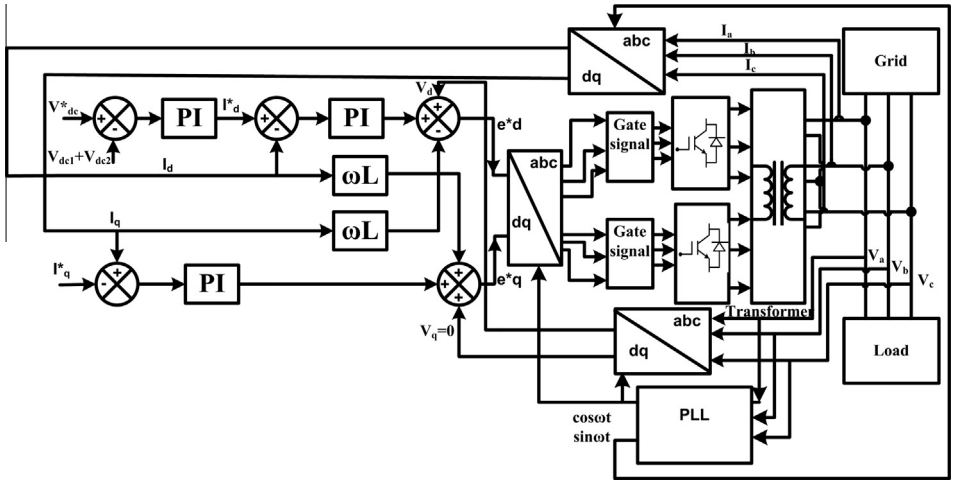

Fig. 6. Control block diagram of scheme-I.

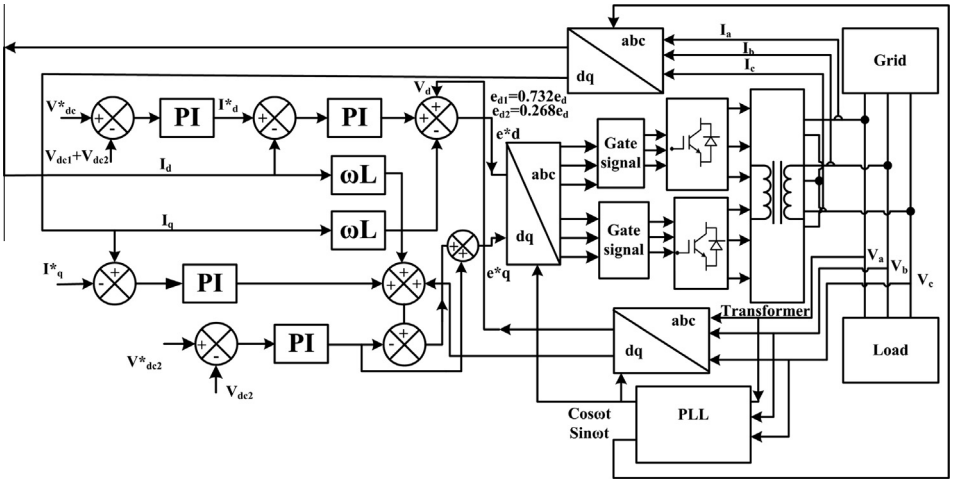

Fig. 7. Control block diagram of scheme-II.

The current controllers for i_d and i_q are designed identically. The bandwidths for the current controllers are taken at 600 Hz, and that of voltage, controller is chosen as 60 Hz. The controllers are tested to operate satisfactorily in the simulation environment. The i_q^* is derived from the amount of reactive power supply to the grid. The DC voltage controller ensures that the available power from the solar PV system be supplied to the grid. Thus, the reduction in solar irradiance will result in a reduction of i_d in the controller.

The "*d*–*q*" to "a–b–c" conversion has been achieved with the standard vector control practice. The first and second inverters are receiving 180° phase shifted modulating signals. The gate signals are generated after comparing them with a triangular carrier wave of switching frequency [22].

CTLI DC-link balance controller

The control scheme-II, adopted for unequal dc link voltages, are shown in Fig. 7 [14]. Additional control is required to regulate individual DC-link voltages of the inverters, $e_I \angle \delta$ is the resulting voltage of the cascaded inverter. Where,

$$e_I = \sqrt{e_d^2 + e_q^2} \tag{14}$$

$$\text{and } \delta = \tan^{-1}((e_q)/(e_d)) \tag{15}$$

The δ can be considered to be proportional to e_q. Accordingly, the *q*-axis reference voltage component of inverters, e_{q1}^*, and e_{q2}^* are found as.

$$e_2^* = (K_P + K_i/S)(V_{dc2}^* - V_{dc2}) \tag{16}$$

$$e_{q1}^* = e_q^* - e_{q2}^* \tag{17}$$

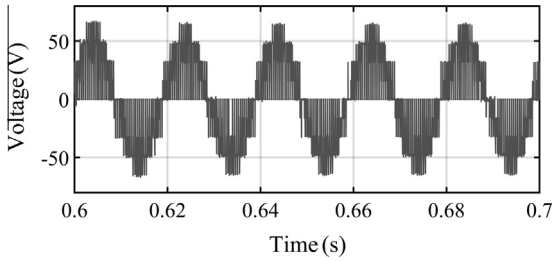

Fig. 8. The cascaded inverter output voltage under the scheme-I.

The DC-link voltages of the inverters are taken as,

$$V_{dc1} = 0.732 V_{dc} \tag{18}$$

$$V_{dc2} = 0.268 V_{dc} \tag{19}$$

Accordingly the reference value of *d*-axis voltage component, e_d^*, is divided in proportion to their respective DC-link voltage as

$$e_{d1}^* = 0.732 e_d^* \tag{20}$$

$$e_{d2}^* = 0.268 e_d^* \tag{21}$$

Phase lock loop (PLL)

The phase-locked loop (PLL) technique is used in the grid-based PV system inverters, mainly for grid synchronization [23,24]. The PLL generates unit signal $\sin \omega t$ and $\cos \omega t$, using source three phase voltages.

System description

The complete scheme, as shown in Fig. 1, is using a transformer with parameters as [13] (see Table 1):

The nature of deviations of solar irradiance level (in percentage), for the two inverters has been presented in Fig. 2(a) and (b). At 0.3 s, the solar irradiance level decreases by 17.133% for the first inverter input. The solar irradiance level is brought back to the rated value at 0.6 s; Fig. 2(b) depicts that the solar irradiance level for second inverter is increases by 17.133% at 0.9 s, and brought back to the normal value at 1.2 s.

The transient behavior of different internal variables of the system, are presented in next section.

Table 1
Transformer parameters.

Parameter	Value
Secondary phase voltage (rms)	400 V
Primary phase voltage (rms)	48 V
Frequency	50 Hz
Power	2.5 kV A
Leakage inductance, *L*	13%
Resistance, *R*	3%

Simulation result

The complete grid-connected PV system has been simulated in the MATLAB/Simulink environment.

Scheme-I: With equal DC-link voltages

The five-level output voltage of the inverter is produced at the steady state, and depicted in Fig. 8. The voltage is applied across the open winding side of the transformer. The higher voltage side of the transformer is directly connected to the grid-connected load.

The active power supplied by the inverters via the transformer can be expressed as:

$$P = \frac{3}{2} i_d V_d \tag{22}$$

The V_d is found constant in the considered reference frame. Hence, the active power is directly proportional to the magnitude of i_d.

The transient behavior of the total DC-link voltage, direct axis and quadrature axis component of the PV system output current has been presented in Fig. 9. The variables are adjusted by the controller successfully, to maintain the DC-link voltage level at the desired level; 96 V. Undershoots and overshoots are observed in the DC-link voltage waveform, because of the step changes in the irradiance level. However, the controller brings the voltage back to the reference level, within 0.1 s in each case. The i_d has decreased to 4.23 A from the initial value of 5 A, due to the reduction in the solar irradiance level. This reduction in i_d was to maintain the DC-link voltage at the desired level by reducing the power flow from the PV system. The i_q is kept constant at zero to ensure no reactive power exchange with the PV system at daytime. This ensures maximum utilization of the available solar power. Later, the i_d is found to be increased up to 5.58 A, because of the increment in solar irradiance level.

Scheme II: With unequal DC-link voltages

The output voltages of the inverters are found to be of higher level (seven level), as expected because of the choice of DC-link voltages of the inverters, respectively at 70.272 V and 25.728 V. The output voltage waveform is shown in Fig. 10.

The variations of the solar irradiance level for the inverters are kept same as the earlier scheme. The transient behavior of the total DC-link voltage, direct axis and quadrature axis component of the PV system output current has been presented in Fig. 11(a) and (b) The variables are adjusted by the controller successfully, to maintain the total DC-link voltage level at the desired level; 96 V. Undershoots and overshoots are observed in the DC-link voltage waveform, because of the step changes in the input solar irradiance level for the first inverter. However, the controller brings the voltage back to the reference level, within 0.1 s in each case. In this scheme the DC-link voltage does not change significantly during the variation of the input solar irradiance level for the second inverter.

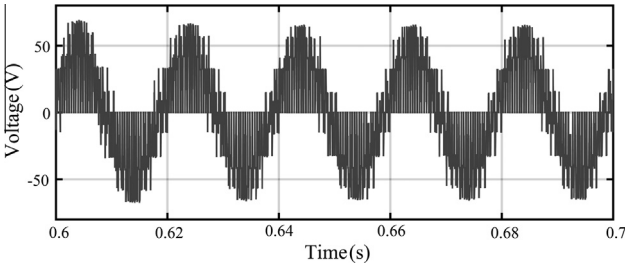

Fig. 10. The cascaded inverter output voltage under the scheme-II.

The i_d has decreased to 3.79 A from the initial value of 5 A, due to the reduction in the solar irradiance level. This reduction in i_d was to maintain the DC-link voltage at the desired level by reducing the power flow from the PV system. The i_q is kept constant at zero to ensure no reactive power exchange with the PV system at daytime. This ensures maximum utilization of the available solar power. It is interesting to note that due to increase in solar irradiance in second inverter, the direct axis current changes by the small amount in its magnitude. This signifies that, the power delivery has small change unlike scheme-I, for variation of solar irradiance level for the low-power PV module. The change in the quadrature axis current during the entire operation is found to be negligible.

Reactive power control

The grid-connected PV systems, with available solar irradiance, are connected to the CTLI to produce active power. In this paper, the proposed control scheme enables the PV systems to work in distributed static reactive power compensator (DSTATCOM) mode, in the absence of solar irradiance.

Considering $V_q = 0$ the reactive power of the system can be calculated as:

$$Q = -\frac{3}{2}(i_q V_d) \tag{23}$$

For lagging reactive power supply the i_q is going to have some negative value. The reference value for i_q has to be generated, following the capacitor, and inverter ratings. In this case, the lagging reactive power supply is increased by 1700 V A in a step, in the absence of solar irradiance. The command is given at 1.5 s in the simulation. The effect, for the scheme-I, has been presented in Fig. 12. The i_q is shown to reach the required level of −3.5 A, to supply the reactive power. The i_d is found to be zero, signifying the fact that no active power is being supplied in the absence of solar power.

However, because of a sudden change in reactive power supply, the capacitors draw some currents from the grid, and the losses are increasing, due to increase in the current supplied by the grid. It is found that the i_d takes 15 ms to be stable. The nature of variation in the DC-link voltage is depicted in Fig. 12(b). It takes 0.04 s to be

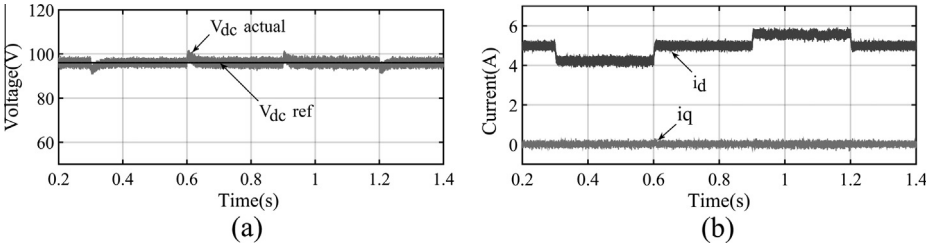

Fig. 9. Response to changes in solar irradiance in the cascaded inverter under the scheme-I (a) combined DC-link voltage, and (b) direct axis and quadrature axis current.

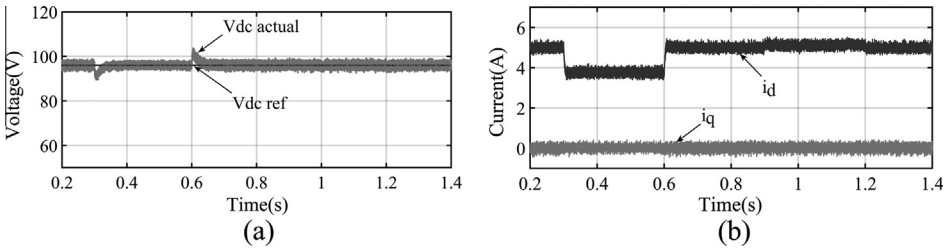

Fig. 11. The CTLI in response to the reduction of solar irradiance under the scheme-II (a) combined DC-link voltage, and (b) direct axis and quadrature axis current.

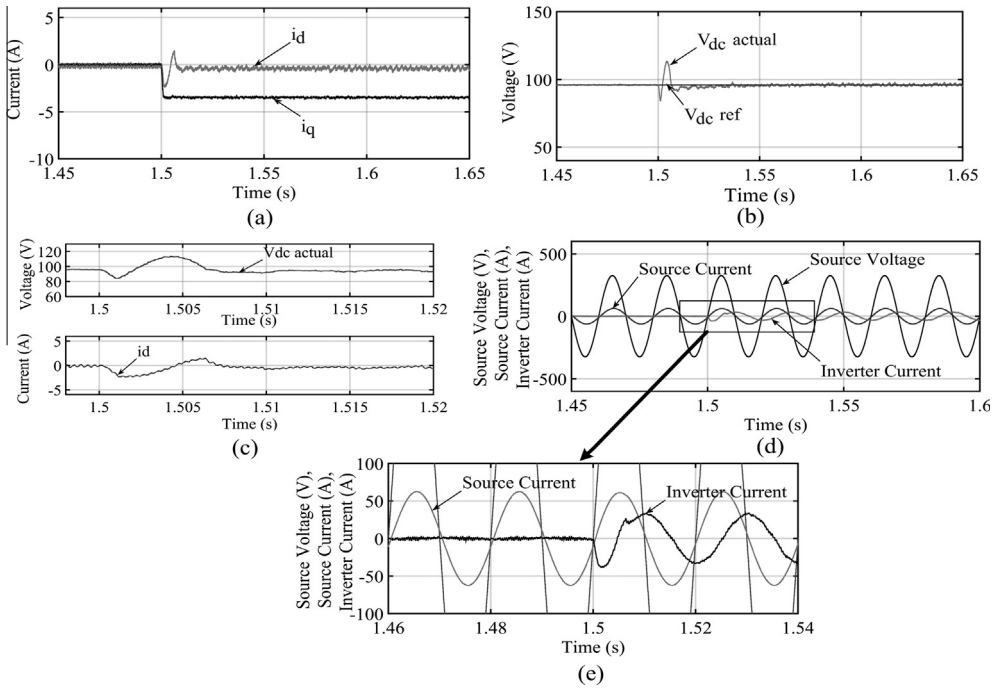

Fig. 12. The CTLI, with the increase in the reactive power supply in DSTATCOM mode under the scheme-I, (a) direct axis and quadrature axis current, (b) DC-link voltage, (c) the nature of change in id to bring the dc link voltage back to its reference value, (d) the source voltage, source current and inverter current, and (e) zoomed view.

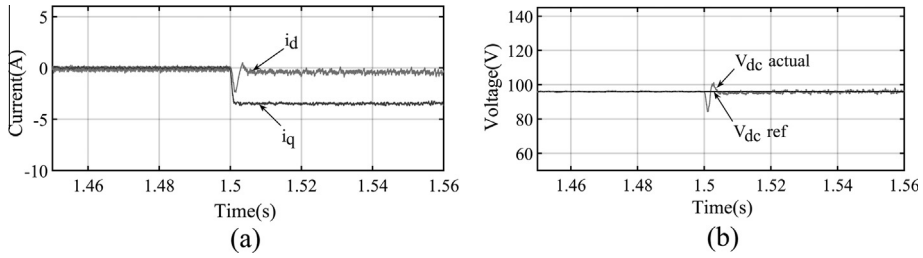

Fig. 13. The CTLI, with the increase in the reactive power supply in DSTATCOM mode under the scheme-II, (a) direct axis and quadrature axis current, and (b) DC-link voltage.

stabilized. The dc link voltage controller successfully maintains the DC-link voltage by balancing the power flow across the capacitor. Similar changes are observed for the scheme-II. The nature of the previously discussed variables is shown in Fig. 13 for scheme II.

Hence, it can be mentioned that both the schemes are effective to operate as DSTATCOM in the absence of the solar irradiance.

Output power and efficiency of the schemes

The active power supplied by the grid-connected PV system is given by Eq. (22). The DC power input to the individual inverters can be calculated following,

$$P_i = V_{dc\_i} I_{dc\_i}, \quad i = 1, 2 \tag{24}$$

The total power input to the inverters is $P_T = P_1 + P_2$. The power loss is calculated as $(P_L) = P_T - P$.

$$\text{Hence, } \%P_{Loss} = 100 \times \frac{P_L}{P_T} \tag{25}$$

The powers of the PV systems in response to change of solar irradiance for the scheme-I and scheme-II are presented in Fig. 14(a) and (b). Table 2 presents the power loss of the PV systems in response to change of solar irradiance for the scheme-I and scheme-II.

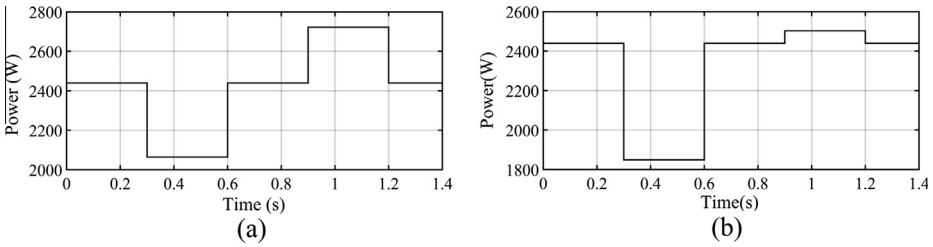

Fig. 14. Power output of the PV System in response to the change of solar irradiance in different time under the (a) SCHEME-I and (b) scheme-II.

Table 2
Solar deviation (%) from nominal value, with power loss.

	Time (s)	Solar deviation (%)	P_1 (W)	P_2 (W)	Active power (P) (W)	Power loss (W)
Scheme-I	0	0	1368	1368	2439.45	296.55
	0.3	−17.133[a]	960	1344	2063.7747	240.23
	0.6	0	1368	1368	2439.45	296.55
	0.9	17.133[b]	1280	1792	2722.4262	349.57
	1.2	0	1368	1368	2439.45	296.55
Scheme-II	0	0	2016	758.44	2439.45	334.99
	0.3	−17.133[a]	1430	617.4	1849.1031	198.05
	0.6	0	2016	750.4	2439.45	326.45
	0.9	17.133[b]	1997	840.75	2502.8757	334.47
	1.2	0	2018	744.8	2439.45	323.75

[a] For inverter I.
[b] For inverter II.

It is found that the power loss of the system with the initial solar irradiance level is 10.83%, and the active power delivered is 2439.45 W. The power loss reduces to 10.4% with reduction in solar irradiance level at first inverter. The delivered active power is also found to be reduced to 2063.77 W. The power loss increases to 11.38% with increment in solar irradiance level in second inverter. The delivered active power is found to be increased to 2722.43 W.

In scheme II, on the other hand the initial power loss is found to be 12.074%. It has reduced to 9.67% with reduction in solar irradiance at the first inverter. The delivered active power is found to be reduced to1849.1 W. Though the delivered active power increased by a very small amount in response to the increment in solar irradiance at second inverter, the power loss is found to be increased to 11.78%.

The efficiency of the considered CTLI based systems for both the schemes are coming close to 90%. Thus, the present system is found to be increasing the range of operation, for solar irradiance levels, maintaining the efficiency at the level of prevailing power schemes [25].

Harmonic analysis of the schemes

The values of the THD of the output current for the proposed schemes are computed using Eq. (26).

$$\%THD_i = 100 \times \sqrt{\sum_{h\neq 1}\left(\frac{I_{sh}}{I_{s1}}\right)^2} \tag{26}$$

where the subscript i indicates the THD in current, I_{s1} is the fundamental (line-frequency f_1) component, I_{sh} is the component at the h harmonic frequency ($f_h = hf_1$).

The transformer output currents for the proposed scheme-I and scheme-II are presented in Figs. 15(a) and 16(a) respectively. The harmonic spectrums of these currents are shown in Figs. 15(b) and 16(b). The THD, generated by scheme-I and scheme-II, are found to be 2.96% and 3.89% only. The lower-order harmonics are almost reduced to negligible value in these schemes.

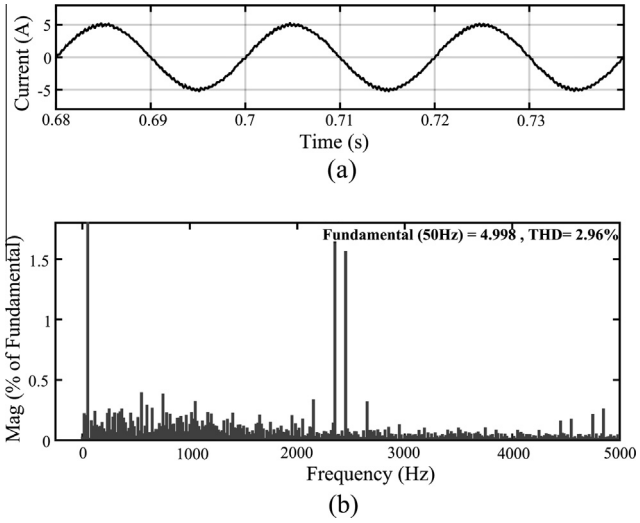

Fig. 15. For proposed scheme I: (a) transformer output current (b) harmonic spectrum of the current.

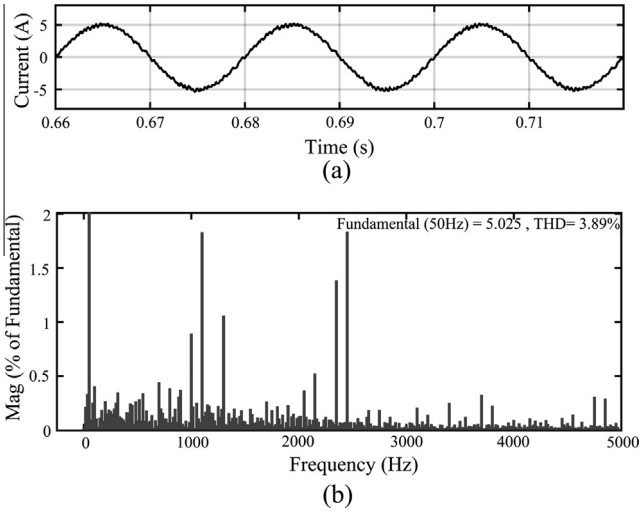

Fig. 16. For proposed scheme II: (a) transformer output current (b) harmonic spectrum of the current.

A comparison with some of the existing PV systems with the proposed schemes is shown in Table 3. From this table, it can be concluded that the proposed scheme is advantageous in most of the attributes while it is comparable in the remaining attributes.

Table 3
Comparison of the proposed scheme with some of the existing systems.

Schemes/paper	Pires [5]	Kjaer [26] Type-1	Kjaer [26] Type-2	Babu [14]	Liu [27]	Proposed scheme-I	Proposed scheme-II
Per phase grid voltage	#	230 V	230 V	230 V	120 V	**230 V**	**230 V**
Input voltage	40–50 V	24–40 V	28 V	659 V 241 V	#	**48 V**	**48 V**
Control strategy	SMC	#	#	Vector control	Vector control	**Vector control**	**Vector control**
Inverter type	Three phase	Soladin 120	Modified Shimizu	Three phase	Three phase	**Three phase**	**Three phase**
No. of DC–DC converter	2	#	#	0	4	**0**	**0**
Converter output voltage Level	5	#	#	5	#	**5**	**7**
Applications	PV System	PV System	PV System	STATCOM	PV system/STATCOM	**PV system/STATCOM**	**PV system/STATCOM**
No. of transformer	1	1	1	1	4	**1**	**1**
No. of inductor	0	2	1	0	12	**0**	**0**
No. of capacitors	2	2	3	2	16	**2**	**2**
Efficiency (%)	#	93	87	#	#	**90**	**90**
THD (%)	#	#	#	11.82	3.98	**2.96**	**3.89**

= data not available.
Bold values signifies the results of the present work proposals.

Conclusion

The present work employs a novel vector controlled, CTLI for grid-connected PV systems. The simple PWM technique is used to produce the gate signals in place of prevailing SVPWM technique. Here the performance of the CTLI is found to be satisfactory for two different control schemes. Moreover, both active and reactive power delivery, in presence and absence of solar power, are found to be achieved successfully. The scheme-I consider equal DC-link voltages for both the inverters. On the other hand, the second inverter voltage is kept at 0.366 times the voltage of the first inverter, in scheme-II. This was done to obtain lesser harmonic distortion in the inverter output voltage. The results show good performance of the control schemes in both steady state and transient conditions. The controller is shown to extract maximum power from the solar PV modules by maintaining the DC-link voltage at the desired level for both the schemes. The performances of the controllers, under deviations in the input power to the inverters, due to changes in the availability of the solar irradiance, are found to be satisfactory in nature. It is found that increase in solar power in the scheme-I in any one of the inverters results in more active power delivery. However, under scheme-II, an increase in solar irradiance in the second inverter causes an insignificant rise in the direct axial current. This results in a trivial increase in active power delivery. Moreover, it is interesting to note that in the absence of solar power, both the control schemes act in DSTATCOM mode to supply reactive power to the grid. The performance index of both the systems, especially efficiency and THD, are found to be much improved with respect to the existing schemes. This ensures the utilization of the PV system for both active and reactive power delivery with the different solar power level.

References

[1] Carrasco JM, Franquelo LG, Bialasiewicz JT, Galván E, Guisado RCP, Prats MÁM, et al. Power-electronic systems for the grid integration of renewable energy sources: a survey. IEEE Trans Ind Electron 2006;53(4):1002–16.
[2] Libo Wu, Zhengming Zhao, Jianzheng Liu. A single-stage three-phase grid-connected photovoltaic system with modified MPPT method and reactive power compensation. IEEE Trans Energy Convers 2007;22(4):881–6.
[3] Chaouachi Aymen, Kamel Rashad M, Nagasaka Ken. A novel multi-modal Neuro-fuzzy-based MPPT for three-phase grid-connected photovoltaic system. Sol Energy 2010;84(12):2219–29.
[4] Varma Rajiv K, Khadkikar Vinod, Seethapathy Ravi. Nighttime application of PV solar farm as STATCOM to regulate grid voltage. IEEE Trans Energy Convers 2009;24(4):983–5.
[5] Pires VF, Martins JF, Hao C. Dual-inverter for grid-connected photovoltaic system: modeling and sliding mode control. Sol Energy 2012;86:2106–15.
[6] Kumar N, Saha TK, Dey J. Study on photovoltaic system for isolated and non-isolated source cascaded two level inverter (CTLI). In: Proc IESA-2014; 2014. p. 202–6.
[7] Grandi G, Rossi C, Ostojic D, Casadei D. A new multilevel conversion structure for grid-connected PV applications. IEEE Trans Ind Electron 2009;56(11):4416–26.
[8] Kumar N, Saha TK, Dey J. Cascaded two level inverter based grid connected photovoltaic system: modeling and control. In: IEEE international conference on industrial technology (ICIT)-2014; 2014. p. 468–73.
[9] Kumar N, Saha TK, Dey J, Barman JC. Modelling, control, and performance study of cascaded inverter based grid connected PV system. In: 6th international renewable energy congress (IREC), 24–26 March 2015, Sousse, Tunisia; 2015. p. 1–6.
[10] Rodriguez J, Lai JS, Peng FZ. Multilevel inverters: a survey of topologies, control and applications. IEEE Trans Ind Electron 2002;49(4):724–38.
[11] Tolbert Leon M, Peng Fang Z. Multilevel converters as a utility interface for renewable energy systems. IEEE Power Eng Soc Summer Meeting 2000;2:1271–4.
[12] Gupta KK, Ranjan A, Bhatnagar P, Sahu LK, Jain S. Multilevel inverter topologies with reduced device count: a review. IEEE Trans Power Electron 2016;31(1):135–50.
[13] Babu NNVS, Rao DA, Fernandes BG. Asymmetrical DC link voltage balance of a cascaded two level inverter based STATCOM. In: TENCON 2010 IEEE region 10 conference; 2010. p. 483–8.
[14] Babu NNVS, Fernandes BG. Cascaded two-level inverter-based multilevel STATCOM for high-power applications. IEEE Trans Power Deliv 2014;29(3):993–1001.
[15] Gow JA, Manning CD. Development of a photovoltaic array model for use in power-electronics simulation studies. lEE Proc-Electr Power Appl 1999;146(2):193–200.
[16] Villalva Marcelo Gradella, Gazoli Jonas Rafael, Filho Ernesto Ruppert. Comprehensive approach to modeling and simulation of photovoltaic arrays. IEEE Trans Power Electron 2009;24(5):1198–208.
[17] Barrena JA. Individual voltage balancing strategy for PWM cascaded H-bridge converter-based STATCOM. IEEE Trans Ind Electron 2008;55(1):21–9.
[18] Silva LA, Pimentel SP, Pomilio JA. Analysis and proposal of capacitor voltage control for an asymmetrical cascaded inverter. In: The 36th IEEE power electronics specialists conference, 2005. PESC '05; 2005. p. 809–15.
[19] Mohaptra KK, Gopakumar K, Somasekhar VT. A harmonic elimination and suppression scheme for an open-end winding induction motor drive. IEEE Trans Ind Electron 2003;50(6):1187–98.
[20] Debnath Dipankar, Chatterjee Kishore. Two-stage solar photovoltaic-based stand-alone scheme having battery as energy storage element for rural deployment. IEEE Trans Power Electron 2015;62(7):4148–57.
[21] Tian Hongmei, Mancilla-David Fernando, Ellis Kevin, Muljadi Eduard, Jenkins Peter. A cell-to-module-to-array detailed model for photovoltaic panels. Sol Energy 2012;86:2695–706.
[22] Mohan Ned, Undeland TM, Robbin WP. Power electronics: converters, application and design. John Wiley and Sons; 2009.
[23] Fatu Marius, Tutelea L, Teodorescu R, Blaabjerg F, Boldea I. Motion sensorless bidirectional PWM converter control with seamless switching from power grid to stand alone and back. In: IEEE power electronics specialists conference; 2007. p. 1239–44.
[24] Fatu Marius, Blaabjerg Frede, Boldea Ion. Grid to standalone transition motion-sensor less dual-inverter control of PMSG with asymmetrical grid voltage sags and harmonics filtering. IEEE Trans Power Electron 2014;29(7).
[25] Masaoud Ammar, Ping Hew Wooi, Mekhilef Saad, Taallah Ayoub Suliman. New three-phase multilevel inverter with reduced number of power electronic components. IEEE Trans Power Electron 2014;29(11):6018–29.
[26] Kjaer Soeren Baekhoej, Pedersen John K, Blaabjerg Frede. A review of single-phase grid-connected inverters for photovoltaic modules. IEEE Trans Ind Appl 2005;41(5).
[27] Liu L, Li Hui, Xue Yaosuo, Liu Wenxin. Decoupled active and reactive power control for large-scale grid-connected photovoltaic systems using cascaded modular multilevel converters. IEEE Trans Power Electron 2015;30(1):176–87.